# Rotation-configured topological phase transition in triangle photonic lattices

Chen Chen, Wange Song,[*] Zhiyuan Lin, Shengjie Wu, Shining Zhu, and Tao Li[†]

*National Laboratory of Solid State Microstructures, Key Laboratory of Intelligent Optical Sensing and Manipulations, Jiangsu Key Laboratory of Artificial Functional Materials, College of Engineering and Applied Sciences, Nanjing University, Nanjing 210093, China*

Photonic topological edge states have shown powerful capabilities to manipulate light propagations. In particular, the all-dielectric structures serve as a promising platform to support the topological states, in which the nontrivial photonic band is usually acquired by engineered shape and lattice with isotropic structures. Here, we propose to manipulate the topological phases in two-dimensional (2D) triangle photonic lattices composed of anisotropic pillars. It is found that the rotation of pillars or unit cells, accompanied by complex coupling effects, can infuse degrees of freedom to switch the photonic band structure between trivial and nontrivial topological phases. We further work out a 2D phase diagram describing the rotation-induced topological transition and demonstrate polarization-dependent robust one-way light propagations in silicon at telecommunication wavelength. This work proposes an alternative scheme to manipulate the topological phases and nontrivial photonic states, which promises more interesting explorations of on-chip light manipulation.

## I. INTRODUCTION

Topological photonics has taken on a notable significance in discovering new photonic phases and states, in which the nontrivial photonic bands are investigated analogous to electronic topological insulators [1–3]. The emergence of topological effects is often underlain by adiabatic cyclic variation of a specific set of parameters, which leads to quantized Berry phases in the momentum space that give rise to various types of topological phases [4–8]. In the topologically nontrivial phases, the systems support robust and unidirectional electromagnetic (EM) surface wave propagation immune to scattering, disorders, and defects, enabling entirely new ways to route information for communication and computing [9–24]. In particular, nonmagnetic all-dielectric artificial structures have been proposed to mimic the quantum spin Hall effects [11,12,25–30] and quantum valley Hall effects [9,31–38]. These analog dielectric systems redefine spin/valley degrees of freedom in classical wave setups by tailoring lateral lattice symmetry of the optical lattices [11,28,30,31,39–46]. Note that in previous works, the dielectric structures usually were isotropic cylinders that possess rotational symmetry, while more sophisticated manipulation of the artificial structure may further enrich the modulation of topological phases.

On the other hand, the metasurfaces with subwavelength artificial structures has generated considerable interest in manipulating the light field [47–50]. By exquisitely tailoring the shape [51], symmetry [52], or rotation angle [53] of the metapillars, unprecedented flexible control of the light amplitude, phase, and polarization can be obtained. To be mentioned, besides the geometric (Berry) phase in the momentum space that defines the topological band properties, the geometric-phase effect can be used in controlling light polarization [i.e., Pancharatnam-Berry (PB) phase] by rotating anisotropic pillars in the real spaces [53,54], which serves as one of the powerful methods in light steering with metasurfaces [55–57]. It suggests that the rotation of anisotropic metapillars [58–61] could provide a new design scheme for light manipulation, and probably gives rise to more fruitful photonic topological phase transition.

In this work, we systemically investigate how the rotation of anisotropic structures can control the topological transition of the photonic band structure, and demonstrate the associated nontrivial edge modes in silicon at telecommunication wavelength. Specifically, by replacing the cylindrical pillars with anisotropic rectangular pillars, a formerly trivial band structure can be tuned to be topologically nontrivial according to the inverted *p*- and *d*-type bands. Further rotating the nanostructure would switch the quantized Berry phase between trivial and nontrivial phases. Besides rotating a single pillar, the rotation of the unit cells as a whole [45,46] can also be harnessed to jointly manipulate the topological phases. Importantly, we work out a phase diagram describing the complex topological phase transition of the rotational photonic band structures. We further confirm the emergence of the topologically protected one-way light propagation by interfacing two media with distinct topological phases with respective rotation engineering. This work suggests that the nontrivial topological phase can be acquired by rotating the anisotropic structures without changing the shape or location, which provides degrees of freedom to engineer the topological band structure and control the light propagations.

## II. STRUCTURE AND PRINCIPLE

Figure 1(a) shows the schematics of the dielectric structure arranged in a two-dimensional (2D) triangle lattice composed of six anisotropic dielectric pillars in air (the purple hexagon

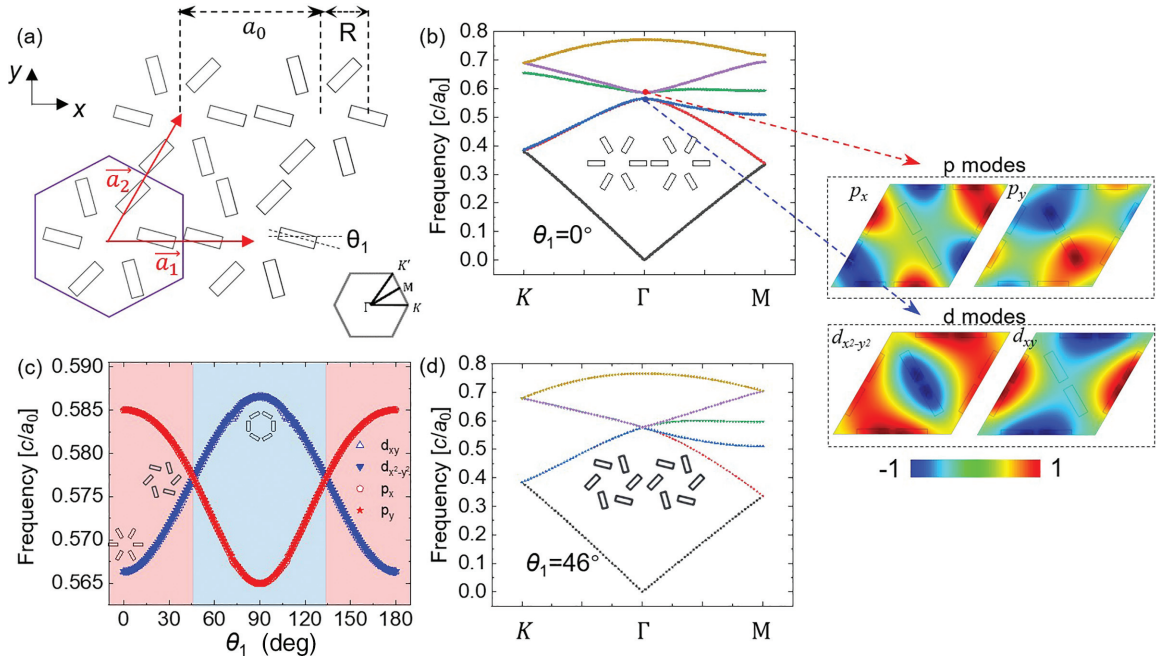*songwange@nju.edu.cn
†taoli@nju.edu.cn

FIG. 1. (a) Schematic diagram of triangle lattice composed of anisotropic dielectric pillars in air, where $a_0$ is lattice constant, $R$ is distance between pillars and center of lattice satisfying $a_0/R = 3$, $\theta_1$ is rotation angle of pillars, and $\boldsymbol{a}_1$ and $\boldsymbol{a}_2$ are primitive vectors. (b) Band structures of lattice for $\theta_1 = 0°$, two right panels correspond to $E_z$ field of two $p$ modes and two $d$ modes, respectively. Inset shows schematics of lattice arrangement. (c) Eigenfrequencies of $p$ modes (red) and $d$ modes (blue) at $\Gamma$ point as function of $\theta_1$. (d) Band structure of lattice for $\theta_1 = 46°$ where double Dirac cone appears. Inset shows schematics of lattice arrangement.

is the unit cell). $\boldsymbol{a}_1$ and $\boldsymbol{a}_2$ are the unit vectors of the lattice and the lattice constant is $a_0$. The distance between the center of each atom to the centroid of each hexagon is $R$, which satisfies $R = a_0/3$. The first Brillouin zone is also shown in Fig. 1(a), with $\Gamma$, $M$, and $K$ indicating the high-symmetry points. We consider the behavior of the transverse magnetic (TM) mode of the EM wave, namely, those of finite out-of-plane $E_z$ and in-plane $H_x$ and $H_y$ components with others being zero. According to Maxwell's equation, the propagation of the TM waves in structure can be described by [11,62]

$$\left[\frac{1}{\varepsilon(\mathbf{r})} \nabla \times \nabla \times\right] E_z(\mathbf{r})\widehat{z} = \frac{\omega^2}{c^2} E_z(\mathbf{r})\widehat{z}, \quad (1)$$

where $\varepsilon(\mathbf{r})$ is the position-dependent permittivity and $c$ is the speed of light. The magnetic field then can be calculated by Faraday's law, $\mathbf{H} = -[i/\mu_0\omega]\nabla \times \mathbf{E}$. Note that different from previous works the pillars are usually cylinders with rotation symmetry and the topological phase transition happens by deforming the lattice [shrinking ($R < a_0/3$) or expanding ($R > a_0/3$)] or changing the radius of the cylinders. Here, the pillar structures are anisotropic; thus, the rotation angle $\theta_1$ of each pillar provides a degree of freedom for topological band manipulation. Specifically, the geometric parameters used in the model are $a_0 = 900$ nm, $w = 78$ nm (width of the pillar), and $l = 238$ nm (length of the pillar). The pillars are silicon with refractive index $n = 3.47$, and the background media is set as air. As a proof of concept, we consider a system infinite in the $z$ direction which reduces the problem to 2D. The underlying physics will preserve in practical 3D structure with a finite thickness [11]. Figure 1(b) shows the dispersion relations of the TM mode computed by a commercial

software COMSOL MULTIPHYSICS based on the finite-element method in the case of $\theta_1 = 0°$ [the structure is illustrated in Fig. 1(b)]. The anisotropic pillars break the double Dirac cone of common cylindrical case at the $\Gamma$ point and result in a band gap opening. There are two double-degeneracy points at the $\Gamma$ point protected by $C_6$ symmetry, which carry $p$-type ($p_x$ and $p_y$) and $d$-type ($d_{xy}$ and $d_{x^2-y^2}$) orbitals with odd- and even-parity symmetry, respectively [see the corresponding $E_z$ field profiles of the two bands in the vicinity of the $\Gamma$ point in the right panel of Fig. 1(b)]. In a photonic structure with $C_6$ symmetry, it is shown that a pseudo–time-reversal symmetry ($T_p$) can be constructed, such that $T_p = -1$ [11], resulting in a Kramers pair, i.e., pseudospin, which is defined as

$$p_\pm = (p_x \pm ip_y)/\sqrt{2}, \quad [d_\pm = (d_{x^2-y^2} \pm id_{xy})/\sqrt{2}]. \quad (2)$$

Here, the two eigenstates of odd (even) parity in $p\pm$ $(d\pm)$ can be mapped as the pseudospin-up and pseudospin-down states for the $p(d)$ band, which could be excited by counterclockwise and clockwise rotations of in-plane magnetic fields, as will be shown later. According to Fig. 1(b), the photonic band below (above) the gap is occupied by $d$-type ($p$-type) states, which is opposite to the order away from the $\Gamma$ point. Therefore, a band inversion takes place that indicates a nontrivial topological phase, which is described by the spin Chern number [11,63].

### III. RESULTS AND DISCUSSION

Note the nontrivial topological phase is achieved by simply replacing the cylinder with anisotropic pillars without
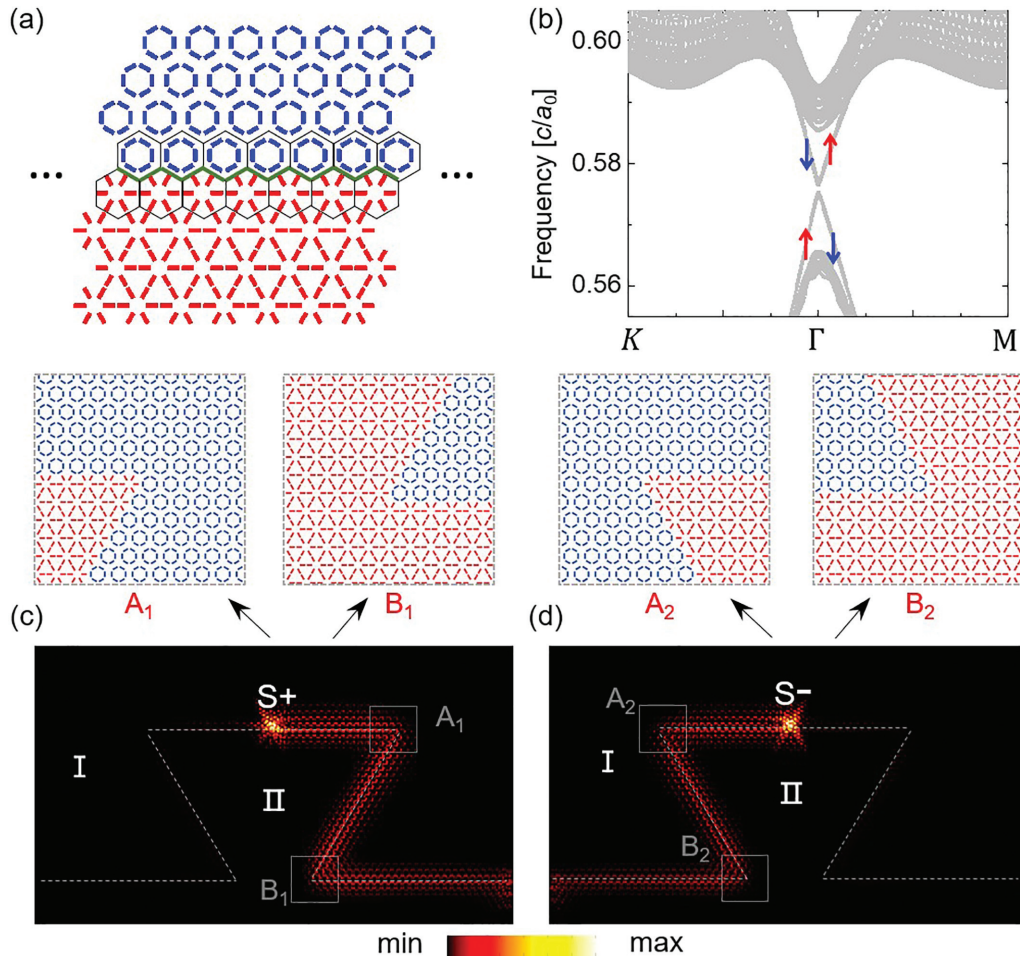
FIG. 2. (a) Illustration of compound lattice with trivial part (blue) and nontrivial part (red) arranged in zigzag configuration. Black frame shows cell shape and green curve marks interface. (b) Projected band diagrams of compound lattice with two distinct structures with $\theta_1 = 0°$ and $\theta_1 = 90°$ arranged in zigzag configuration. (c), (d) Electric-field distributions ($|E|$) of structure which is excited by pseudospin-up mode $S_+$(c), and pseudospin-down mode $S_-$(d), both showing unidirectional EM wave propagation. Gray dashed line indicates zigzag interface. Top panels illustrate specific structures around four sharp corners $A_1$, $B_1$, $A_2$, and $B_2$.

changing the center position. In fact, the band structures and the mode properties can be further modulated by changing the rotating angle $\theta_1$. Figure 1(c) shows the simulated eigenfrequencies of the $p$ modes ($\omega_p$) and $d$ modes ($\omega_d$) at $\Gamma$ point as a function of $\theta_1$. A critical angle for the topological transition is identified at $46°$, where $p$ modes and $d$ modes degenerate with a close band gap resulting from the equivalence of the intra- and intercluster coupling and form a double Dirac cone [see Fig. 1(d)]. When $\theta_1 < 46°$, the $p$-type state has a higher frequency than the $d$-type state ($\omega_p > \omega_d$), indicating a topologically nontrivial phase. When $\theta_1 > 46°$, the band gap reopens, but with a trivial topological phase ($\omega_p < \omega_d$). This change of topological phase is central symmetric about the pillar rotation angle of $90°$ due to its geometrical symmetries. Notably, the topological transition point is expected to be fixed at $\sim 45°$ regardless of the rectangular sizes (see the Appendix).

The hallmark of topological bands is the robust edge states on the interfaces between topologically distinct structures. Figure 2(a) illustrates a compound lattice composed of a trivial part (blue, $\theta_1 = 90°$) and a nontrivial part (red, $\theta_1 = 0°$)

arranged in a zigzag configuration. Figure 2(b) shows the corresponding projected band diagrams. In this situation, a pair of edge states marked by blue and red arrows exist in the bulk band gap, which has opposite group velocities in the crossing region indicating the existence of counterpropagating directional edge states. This pair of edge states is topologically protected by pseudo time reversal (TR) symmetry and can be identified as the spin-up (counterclockwise) and spin-down (clockwise) modes. Due to the symmetry of $C_6$ being damaged to a certain extent at the interface, there is a tiny gap at the $\Gamma$ point, which would get smaller by increasing the period length. Furthermore, we examine the robust one-way propagation of the topological helical edge states by arranging the topological trivial part (I) with $\theta_1 = 90°$ and nontrivial part (II) with $\theta_1 = 0°$ forming a $\Omega$-shaped domain wall [64]. A harmonic line source $\mathbf{S}_\pm = H_0 e^{i\omega t}(\mathbf{e_x} \mp i\mathbf{e_y})$ (where $\mathbf{e}_x$ and $\mathbf{e}_y$ are unit vectors along the $x$ and $y$ directions) is placed parallel to dielectric pillars to inject the EM wave at the interface with the frequency in the topological band gap. The helicity feature of the source corresponds to the direction of the pseudospins and controls the propaga-
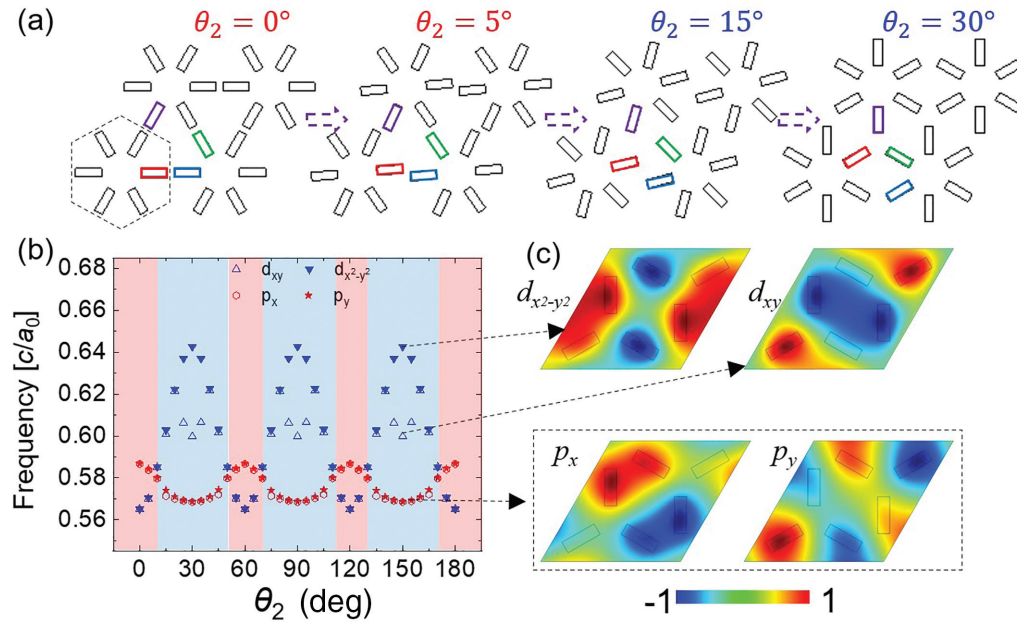
FIG. 3. (a) Schematics of lattice with pillar rotations fixed at $\theta_1 = 0°$ and different unit-cell rotations $\theta_2 = 0°, 5°, 15°$, and $30°$, respectively. (b) Eigenfrequencies of $p$ modes (red) and $d$ modes (blue) at $\Gamma$ point as function of $\theta_2$. (c) $E_z$ field profiles of two $p$ modes (bottom) and two $d$ modes (top) when $\theta_2 = 30°/90°/150°$.

tion of EM waves. As illustrated in Figs. 2(c) and 2(d), the pseudospin-up (pseudospin-down) unidirectional propagation mode is selectively excited with $S_+(S_-)$. The energy is mainly distributed along the sharp domain wall with negligible backscattering, indicating topologically protected propagations.

Besides rotating the pillars ($\theta_1$), the unit cell as a whole can also be synchronously rotated ($\theta_2$) to jointly modulate the topological phase [the rotation schematices are illustrated in Fig. 3(a)]. Without loss of generality, we fix $\theta_1 = 0°$ and show the eigenfrequencies of the $p$ modes ($\omega_p$) and $d$ modes ($\omega_d$) at $\Gamma$ point as a function of $\theta_2$, as shown in Fig. 3(b). It is found that $\omega_p > \omega_d$ when $\theta_2 \Leftarrow 10°$, and $\omega_p < \omega_d$ when $\theta_2 > 10°$, indicating topological transitions from nontrivial to the trivial as $\theta_2$ increases. The topological phase switches back when $\theta_2 > 50°$, which has a cycle of $60°$ according to the $C_6$ symmetry. To be mentioned, when $\theta_2$ is around $30°/90°/150°$, the $d$ modes are no longer degenerate and have a distinct split in eigenfrequencies [see Fig. 3(c)]. This degeneracy breaking might be attributed to the symmetry breaking caused by the rotation, which leads to complex coupling effects (e.g., the red pillar in a unit cell only couples to the one pillar [marked by blue in (a), left panel] in the neighboring unit cell for $\theta_2 = 0$, while it couples to two pillars [marked by the purple and green in (a), right panel] in the neighboring unit cell for $\theta_2 = 30°$).

To obtain a clear physical picture of the topological phase transition caused by the rotations, we systematically analyze the eigenfrequencies of $p$ modes and $d$ modes with different $\theta_1$ and $\theta_2$ to map out a topological phase diagram. As illustrated in Fig. 4(a), the blue regions (I) indicate the trivial phase (spin Chern number $C = 0$) while the red regions (II) are the nontrivial case ($C = 1$). Here, we pick a pair of lattices with topologically trivial region I ($\theta_1 = 30°$, $\theta_2 = 15°$) and nontrivial region II ($\theta_1 = 0°$, $\theta_2 = 0°$)

(marked by golden stars) to form a compound lattice with interface channel for the topologically protected propagating modes. Figure 4(b) shows the projected band diagram of a compound lattice with a zigzag interface. Two topological edge states appear in the bulk band gap and indicate unambiguously counterpropagations of EM energy at the interface associated with two pseudospin states. Then, a $\Omega$-shaped domain wall with topologically trivial region I ($\theta_1 = 30°$, $\theta_2 = 15°$) and nontrivial region II ($\theta_1 = 0°$, $\theta_2 = 0°$) is constructed to demonstrate the robust unidirectional propagation of topological helical edge states. As shown in Figs. 4(c) and 4(d), the harmonic line source $S_+$ and $S_-$ with the frequency in the band gap selectively excites the unidirectional propagation modes with reflectionless light traveling. Taking the topological waveguiding in Fig. 4(c) as an example, the transmission of one sharp corner is calculated about $91 \sim 96\%$, and the unidirectional contrast of the one-way propagation is about 35 dB.

## IV. SUMMARY AND OUTLOOK

In summary, we have investigated the topological properties of a triangle photonic lattice composed of anisotropic rectangles, where the rotation of the structures can serve as an alternative degree of freedom to control the light behaviors. Different from the traditional way of changing the position or size of isotropic cylinders, the joint rotation of the rectangles and the unit cells can construct a 2D phase diagram to illustrate the topological phase transitions. We further verify the emergence of the topological edge states by electromagnetic wave simulations based on silicon in the near-infrared wavelength, which shows polarization-dependent unidirectional propagation along the sharp domain walls.
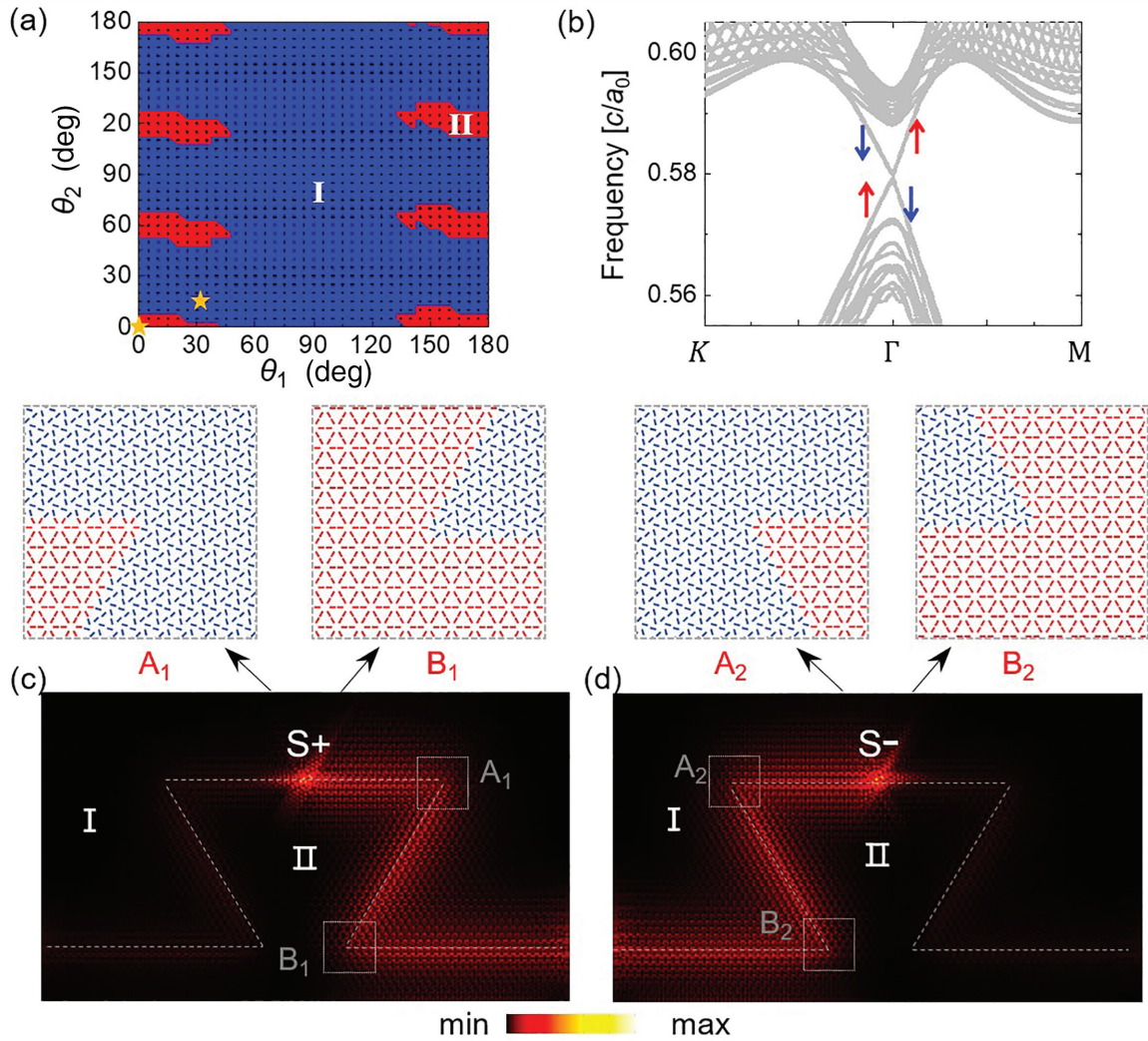
FIG. 4. (a) Topological phase diagram as function of $\theta_1$ and $\theta_2$. Blue region (I) indicates trivial topological phase ($C = 0$) and red region (II) indicates nontrivial topological phase ($C = 1$). (b) Projected band diagram of compound lattice arranged in zigzag configuration, with topologically trivial region I ($\theta_1 = 30°$, $\theta_2 = 15°$) and nontrivial region II ($\theta_1 = 0°$, $\theta_2 = 0°$), marked by stars in (a). (c), (d) Electric-field distributions ($|E|$) of structures with $\Omega$-shaped domain wall excited by pseudospin-up mode $S_+$ (c), and pseudospin-down mode $S_-$ (d). Gray dashed line indicates interface. Top panels illustrate specific structures around four sharp corners $A_1$, $B_1$, $A_2$, and $B_2$.

The artificial nanophotonic structures have shown powerful capabilities for light manipulation in recent years. For example, the PB phase in metasurfaces has been a great success in steering the optical field. In a similar way, though with totally different mechanisms, here we generate the rotation configuration to the topological photonics design in the near-infrared region, which certainly provides dimensions in manipulating photonic topological states. Moreover, considering that the orientation of structures can be well controlled in current nanofabrication technology, our rotation scheme could be more robust against the nanofabrication errors compared to former topological designs such as tuning the size of the nanostructures. Such robust rotation configuration provides design possibilities for achieving more complex photonic edge/corner states [28,46,65–70] for robust on-chip light manipulation, and even could inspire some intriguing effects combined with metasurfaces to extend the light manipulation to free space.

## APPENDIX: ROBUSTNESS OF TOPOLOGICAL TRANSITION ANGLES

The topological transition would be at exactly 45° and 135° (rotation angle of rectangles) due to symmetry considerations in such rectangular cases (leads to the equivalence of the intra- and intercluster coupling), while because of the limited simulation precision, there would be a little deviation ($\leqslant 1°$)
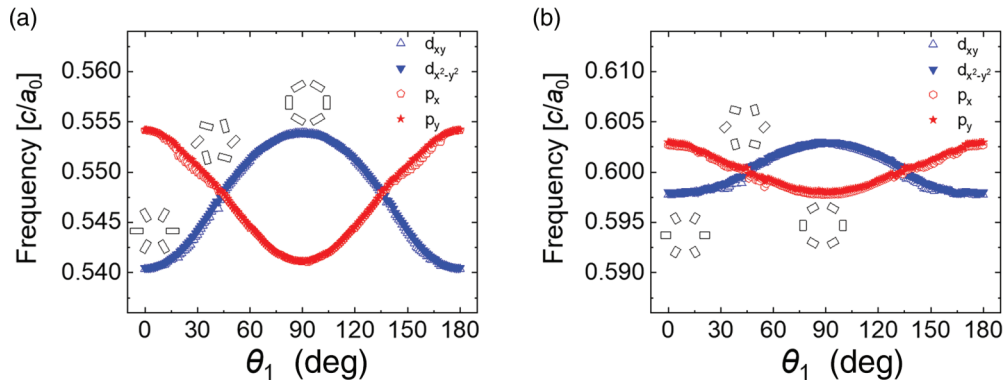
FIG. 5. Eigenfrequencies of $p$ modes (red) and $d$ modes (blue) at $\Gamma$ point as a function of $\theta_1$ when $\theta_2 = 0°$. (a) is the results of the rectangle with $w = 100$ nm and $l = 210$ nm; (b) is the results of the rectangle with $w = 100$ nm and $l = 150$ nm. The insert shows the schematics of the lattice arrangement.

from the expected values. Moreover, the topological transition point is robust with the rectangular sizes. As shown in Fig. 5, although the rectangles have different geometric parameters and aspect ratios [Fig. 5(a) is $w = 100$ nm and $l = 210$ nm; Fig. 5(b) is $w = 100$ nm and $l = 150$ nm], the $p$-$d$ band in-

version still occurs at nearly $45°$ and $135°$, consistent with the results shown in Fig. 1(c) ($w = 78$ nm and $l = 238$ nm). The specific geometric sizes only affect the working frequency, while they do not change the topological transition point.

[1] T. Ozawa, H. M. Price, A. Amo, N. Goldman, M. Hafezi, L. Lu, M. C. Rechtsman, D. Schuster, J. Simon, O. Zilberberg, and I. Carusotto, Topological photonics, Rev. Mod. Phys. **91**, 015006 (2019).

[2] L. Lu, J. D. Joannopoulos, and M. Soljačić, Topological photonics, Nat. Photon. **8**, 821 (2014).

[3] A. B. Khanikaev, S. H. Mousavi, W.-K. Tse, M. Kargarian, A. H. MacDonald, and G. Shvets, Photonic topological insulators, Nat. Mater. **12**, 233 (2013).

[4] L. Fu and C. L. Kane, Topological insulators with inversion symmetry, Phys. Rev. B **76**, 045302 (2007).

[5] M. Z. Hasan and C. L. Kane, Topological insulators, Rev. Mod. Phys. **82**, 3045 (2010).

[6] X.-L. Qi and S.-C. Zhang, Topological insulators and superconductors, Rev. Mod. Phys. **83**, 1057 (2011).

[7] C. L. Kane and E. J. Mele, Quantum spin Hall effect in graphene, Phys. Rev. Lett. **95**, 226801 (2005).

[8] L. Fu, Topological crystalline insulators, Phys. Rev. Lett. **106**, 106802 (2011).

[9] X. T. He, E. T. Liang, J. J. Yuan, H. Y. Qiu, X. D. Chen, F. L. Zhao, and J. W. Dong, A silicon-on-insulator slab for topological valley transport, Nat. Commun. **10**, 872 (2019).

[10] M. I. Shalaev, W. Walasik, A. Tsukernik, Y. Xu, and N. M. Litchinitser, Robust topologically protected transport in photonic crystals at telecommunication wavelengths, Nat. Nanotechnol. **14**, 31 (2019).

[11] L. H. Wu and X. Hu, Scheme for achieving a topological photonic crystal by using dielectric material, Phys. Rev. Lett. **114**, 223901 (2015).

[12] Y. Yang, Y. F. Xu, T. Xu, H.-X. Wang, J.-H. Jiang, X. Hu, and Z. H. Hang, Visualization of a unidirectional electromagnetic waveguide using topological photonic crystals made of dielectric materials, Phys. Rev. Lett. **120**, 217401 (2018).

[13] X. Cheng, C. Jouvaud, X. Ni, S. H. Mousavi, A. Z. Genack, and A. B. Khanikaev, Robust reconfigurable electromagnetic pathways within a photonic topological insulator, Nat. Mater. **15**, 542 (2016).

[14] K. Fang, Z. Yu, and S. Fan, Realizing effective magnetic field for photons by controlling the phase of dynamic modulation, Nat. Photon. **6**, 782 (2012).

[15] M. Hafezi, E. A. Demler, M. D. Lukin, and J. M. Taylor, Robust optical delay lines with topological protection, Nat. Phys. **7**, 907 (2011).

[16] M. C. Rechtsman, J. M. Zeuner, Y. Plotnik, Y. Lumer, D. Podolsky, F. Dreisow, S. Nolte, M. Segev, and A. Szameit, Photonic Floquet topological insulators, Nature (London) **496**, 196 (2013).

[17] W. Song, W. Sun, C. Chen, Q. Song, S. Xiao, S. Zhu, and Tao Li, Breakup and recovery of topological zero modes in finite non-Hermitian optical lattices, Phys. Rev. Lett. **123**, 165701 (2019).

[18] S. Xia, D. Kaltsas, D. Song, I. Komis, J. Xu, A. Szameit, H. Buljan, K. G. Makris, and Z. Chen, Nonlinear tuning of PT symmetry and non-Hermitian topological states, Science **372**, 72 (2021).

[19] H. Zhao, X. Qiao, T. Wu, B. Midya, S. Longhi, and L. Feng, Non-Hermitian topological light steering, Science **365**, 1163 (2019).

[20] L. Yang, G. Li, X. Gao, and L. Lu, Topological-cavity surface-emitting laser, Nat. Photon. **16**, 279 (2022).

[21] Z.-K. Shao, H.-Z. Chen, S. Wang, X.-R. Mao, Z.-Q. Yang, S.-L. Wang, X.-X. Wang, X. Hu, and R.-M. Ma, A high-performance topological bulk laser based on band-inversion-induced reflection, Nat. Nanotechnol. **15**, 67 (2020).

[22] F. D. Haldane and S. Raghu, Possible realization of directional optical waveguides in photonic crystals with broken time-reversal symmetry, Phys. Rev. Lett. **100**, 013904 (2008).

[23] Z. Wang, Y. D. Chong, J. D. Joannopoulos, and M. Soljačić, Reflection-free one-way edge modes in a gyromagnetic photonic crystal, Phys. Rev. Lett. **100**, 013905 (2008).

[24] Z. Wang, Y. Chong, J. D. Joannopoulos, and M. Soljačić, Observation of unidirectional backscattering-immune topological electromagnetic states, Nature (London) **461**, 772 (2009).

[25] S. Peng, N. J. Schilder, X. Ni, J. Van De Groep, M. L. Brongersma, A. Alù, A. B. Khanikaev, H. A. Atwater, and A. Polman, Probing the band structure of topological silicon photonic lattices in the visible spectrum, Phys. Rev. Lett. **122**, 117401 (2019).

[26] S. Barik, H. Miyake, W. DeGottardi, E. Waks, and M. Hafezi, Two-dimensionally confined topological edge states in photonic crystals, New J. Phys. **18**, 113013 (2016).

[27] M. A. Gorlach, X. Ni, D. A. Smirnova, D. Korobkin, D. Zhirihin, A. P. Slobozhanyuk, P. A. Belov, A. Alu, and A. B. Khanikaev, Far-field probing of leaky topological states in all-dielectric metasurfaces, Nat. Commun. **9**, 909 (2018).

[28] B. Xie, G. Su, H. F. Wang, F. Liu, L. Hu, S. Y. Yu, P. Zhan, M. H. Lu, Z. Wang, and Y. F. Chen, Higher-order quantum spin Hall effect in a photonic crystal, Nat. Commun. **11**, 3768 (2020).

[29] D. Smirnova, S. Kruk, D. Leykam, E. Melik-Gaykazyan, D.-Y. Choi, and Y. Kivshar, Third-harmonic generation in photonic topological metasurfaces, Phys. Rev. Lett. **123**, 103901 (2019).

[30] N. Parappurath, F. Alpeggiani, L. Kuipers, and E. Verhagen, Direct observation of topological edge states in silicon photonic crystals: Spin, dispersion, and chiral routing, Sci. Adv. **6**, eaaw4137 (2020).

[31] J.-W. Dong, X.-D. Chen, H. Zhu, Y. Wang, and X. Zhang, Valley photonic crystals for control of spin and topology, Nat. Mater. **16**, 298 (2017).

[32] X.-D. Chen, F.-L. Zhao, M. Chen, and J.-W. Dong, Valley-contrasting physics in all-dielectric photonic crystals: Orbital angular momentum and topological propagation, Phys. Rev. B **96**, 020202(R) (2017).

[33] F. Gao, H. Xue, Z. Yang, K. Lai, Y. Yu, X. Lin, Y. Chong, G. Shvets, and B. Zhang, Topologically protected refraction of robust kink states in valley photonic crystals, Nat. Phys. **14**, 140 (2017).

[34] T. Ma and G. Shvets, All-Si valley-Hall photonic topological insulator, New J. Phys. **18**, 025012 (2016).

[35] O. Jamadi, E. Rozas, G. Salerno, M. Milićević, T. Ozawa, I. Sagnes, A. Lemaître, L. L. Gratiet, A. Harouri, I. Carusotto, J. Bloch, and A. Amo, Direct observation of photonic Landau levels and helical edge states in strained honeycomb lattices, Light Sci. Appl. **9**, 144 (2020).

[36] M. Bellec, C. Poli, U. Kuhl, F. Mortessagne, and H. Schomerus, Observation of supersymmetric pseudo-Landau levels in strained microwave graphene, Light Sci. Appl. **9**, 146 (2020).

[37] C. A. Rosiek, G. Arregui, A. Vladimirova, M. Albrechtsen, B. V. Lahijani, R. E. Christiansen, and S. Stobbe, Observation of strong backscattering in valley-Hall photonic topological interface modes, Nat. Photon. **17**, 386 (2023).

[38] M. C. Rechtsman, Reciprocal topological photonic crystals allow backscattering, Nat. Photon. **17**, 383 (2023).

[39] Y. Wei, B. Yan, Y. Peng, A. Shi, D. Zhao, R. Peng, Y. Xiang, and J. Liu, Fragile topology in double-site honeycomb lattice photonic crystal, Opt. Lett. **46**, 3941 (2021).

[40] Z. Li, H.-C. Chan, and Y. Xiang, Fragile topology based helical edge states in two-dimensional moon-shaped photonic crystals, Phys. Rev. B **102**, 245149 (2020).

[41] X. Zhu, H.-X. Wang, C. Xu, Y. Lai, J.-H. Jiang, and S. John, Topological transitions in continuously deformed photonic crystals, Phys. Rev. B **97**, 085148 (2018).

[42] B. Yan, J. Xie, E. Liu, Y. Peng, R. Ge, J. Liu, and S. Wen, Topological edge state in the two-dimensional Stampfli-triangle photonic crystals, Phys. Rev. Appl. **12**, 044004 (2019).

[43] L. Xu, H.-X. Wang, Y.-D. Xu, H.-Y. Chen, and J.-H. Jiang, Accidental degeneracy in photonic bands and topological phase transitions in two-dimensional core-shell dielectric photonic crystals, Opt. Express **24**, 18059 (2016).

[44] T. Ma and G. Shvets, Scattering-free edge states between heterogeneous photonic topological insulators, Phys. Rev. B **95**, 165102 (2017).

[45] R. Zhou, H. Lin, Y. Liu, X. Shi, R. Tang, Y. Wu, and Z. Yu, Topological edge states of Kekulé-type photonic crystals induced by a synchronized rotation of unit cells, Phys. Rev. A **104**, L031502 (2021).

[46] R. Zhou, H. Lin, Y. Wu, Z. Li, Z. Yu, Y. Liu, and D.-H. Xu, Higher-order valley vortices enabled by synchronized rotation in a photonic crystal, Photon. Res. **10**, 1244 (2022).

[47] N. Yu, P. Genevet, M. A. Kats, F. Aieta, J. P. Tetienne, F. Capasso, and Z. Gaburro, Light propagation with phase discontinuities: Generalized laws of reflection and refraction, Science **334**, 333 (2011).

[48] H. Kwon, D. Sounas, A. Cordaro, A. Polman, and A. Alù, Nonlocal metasurfaces for optical signal processing, Phys. Rev. Lett. **121**, 173004 (2018).

[49] S. Zhang, H. Zhou, B. Liu, Z. Su, and L. Huang, Recent advances and prospects of optical metasurfaces, ACS Photonics **10**, 2045 (2023).

[50] S. M. Kamali, E. Arbabi, A. Arbabi, and A. Faraon, A review of dielectric optical metasurfaces for wavefront control, Nanophotonics **7**, 1041 (2018).

[51] A. Arbabi, Y. Horie, M. Bagheri, and A. Faraon, Dielectric metasurfaces for complete control of phase and polarization with subwavelength spatial resolution and high transmission, Nat. Nanotechnol. **10**, 937 (2015).

[52] C. Chen, S. Gao, W. Song, H. Li, S.-N. Zhu, and T. Li, Metasurfaces with planar chiral meta-atoms for spin light manipulation, Nano Lett. **21**, 1815 (2021).

[53] L. Huang, X. Chen, H. Mühlenbernd, G. Li, B. Bai, Q. Tan, G. Jin, T. Zentgraf, and S. Zhang, Dispersionless phase discontinuities for controlling light propagation, Nano Lett. **12**, 5750 (2012).

[54] S. Pancharatnam, Generalized theory of interference, and its applications, Proc. Indiana Acad. Sci. A **44**, 247 (1956).

[55] C. Chen, W. Song, J.-W. Chen, J.-H. Wang, Y. H. Chen, B. Xu, M.-K. Chen, H. Li, B. Fang, J. Chen, H. Y. Kuo, S. Wang, D. P. Tsai, S. Zhu, and T. Li, Spectral tomographic imaging with aplanatic metalens, Light Sci. Appl. **8**, 99 (2019).

[56] W. Zhuo, S. Sun, Q. He, and L. Zhou, A review of high-efficiency Pancharatnam–Berry metasurfaces, Terahertz Sci. Technol. **13**, 73 (2020).

[57] Y. Guo, M. Pu, F. Zhang, M. Xu, X. Li, X. Ma, and X. Luo, Classical and generalized geometric phase in electromagnetic metasurfaces, Photonics Insights **1**, R03 (2022).

[58] A. Overvig, N. F. Yu, and A. Alù, Chiral quasi-bound states in the continuum, Phys. Rev. Lett. **126**, 073001 (2021).

[59] M. Kang, L. Mao, S. Zhang, M. Xiao, H. Xu, and C. T. Chan, Merging bound states in the continuum by harnessing higher-order topological charges, Light Sci. Appl. **11**, 228 (2022).

[60] J. Chen, H. Huang, S. Huo, Z. Tan, X. Xie, J. Cheng, and G. L. Huang, Self-ordering induces multiple topological transitions for in-plane bulk waves in solid phononic crystals, Phys. Rev. B **98**, 014302 (2018).

[61] H. Huang, S. Huo, and J. Chen, Reconfigurable topological phases in two-dimensional dielectric photonic crystals, Cryst. **9**, 221 (2019).

[62] F. J. D. Joannopoulos, S. G. Johnson, J. N. Winn, and R. D. Meade, *Photonic Crystals: Molding the Flow of Light* (Princeton University Press, Princeton, NJ, 2008).

[63] S.-Q. Shen, *Topological Insulators: Dirac Equation in Condensed Matters*, 2nd ed. (Springer-Verlag, Berlin, 2017).

[64] W. Liu, M. Hwang, Z. Ji, Y. Wang, G. Modi, and R. Agarwal, $Z_2$ Photonic topological insulators in the visible wavelength range for robust nanoscale photonics, Nano Lett. **20**, 1329 (2020).

[65] M. Kim, Z. Jacob, and J. Rho, Recent advances in 2D, 3D and higher-order topological photonics, Light Sci. Appl. **9**, 130 (2020).

[66] S. S. Kruk, W. Gao, D. Y. Choi, T. Zentgraf, S. Zhang, and Y. Kivshar, Nonlinear imaging of nanoscale topological corner states, Nano. Lett. **21**, 4592 (2021).

[67] M. Proctor, P. A. Huidobro, B. Bradlyn, M. B. de Paz, M. G. Vergniory, D. Bercioux, and A. García-Etxarri, Robustness of topological corner modes in photonic crystals, Phys. Rev. Res. **2**, 042038(R) (2020).

[68] B.-Y. Xie, H.-F. Wang, H.-X. Wang, X.-Y. Zhu, J.-H. Jiang, M.-H. Lu, and Y.-F. Chen, Second-order photonic topological insulator with corner states, Phys. Rev. B **98**, 205147 (2018).

[69] W. A. Benalcazar, T. Li, and T. L. Hughes, Quantization of fractional corner charge in Cn-symmetric higher order topological crystalline insulators, Phys. Rev. B **99**, 245151 (2019).

[70] C. W. Peterson, T. Li, W. A. Benalcazar, T. L. Hughes, and G. Bahl, A fractional corner anomaly reveals higher-order topology, Science **368**, 1114 (2020).